Modeling and Simulation of Earthquake Soil Structure Interaction Excited by Inclined Seismic Waves

Hexiang Wang[a], Han Yang[a], Yuan Feng[a], Boris Jeremić[a,b,*]

[a] *Department of Civil and Environmental Engineering, University of California, Davis, CA, USA*

[b] *Environmental and Earth Sciences Area, Lawrence Berkeley National Laboratory, Berkeley, CA, USA*

Abstract

Presented is an application of wave potential formulation (WPF) together with domain reduction method (DRM) to modeling earthquake soil structure interaction (ESSI) behavior in horizontally layered ground under inclined incident seismic waves. Wave potential formulation is used to develop a spatially varying, inclined seismic wave field from incident Primary (P) and Secondary (S) waves that propagate through layered ground. Developed seismic wave field is then used to develop effective forces for Domain Reduction Method that are then used for analyzing ESSI response of a soil structure system. Developed methodology, called WPF-DRM, is verified using analytic solution for a free field response of layered ground subjected to inclined incident waves.

Developed WPF-DRM methodology is illustrated through analysis of an ESSI response of a deeply embedded structure, a small modular reactor (SMR) subjected to incident S wave polarized in vertical plane (SV) with variation in inclinations and frequencies. Presented example highlights the

*Corresponding author

Email address: jeremic@ucdavis.edu (Boris Jeremić)

influences of incident wave inclination and frequency on ESSI response of a deeply embedded structure.
Keywords: earthquake soil structure interaction, deeply embedded structure, inclined incident P/SV/SH waves, layered ground, small modular reactor

Contents

1. Introduction

It has been recognized that during earthquakes, inclined body waves and surface waves have significant influence on a dynamic response of soil structure interaction (SSI) systems [1–5]. For example, incident secondary (S) waves, where soil/rock particles move in horizontal plane (SH), can cause torsional response of structures, Similarly, incident primary (P) and secondary (S) waves, where particles move in vertical plane (SV), can produce amplified rocking of structures, especially in near-fault regions and for structures with large-plan dimensions or multiple supports [6]. Earthquake Soil Structure Interaction (ESSI) response due to inclined incident seismic waves (i.e., P, SH and SV waves) is of significant interest in earthquake engineering.

The Earthquake Soil Structure Interaction problem has been studied for a long time. Early work was focused on dividing an SSI problem into simpler problems that were manageable with available methodology and tools. Substructure method [7] was established to decompose the SSI problem into three sub-problems:

- Free field seismic motion
- Foundation input motion, i.e. foundation wave scattering and impedance function, and
- Superstructure dynamic response

Luco and Wong [8] studied dynamic response of SSI system under non-vertically incident SH wave. SSI responses excited by in-plane wave (P, SV and Rayleigh waves) were presented by Todorovska and Trifunac [9], Todorovska [10]. Effects of site dynamic characteristics on SSI were systematically investigated by Liang et al. [11, 12] for incident P, SV and SH waves.

Due to the limitation of substructure method and the complexity of SSI problem, simplifications have been commonly made in many studies. For example, underground is usually simplified as homogeneous half space or a single homogeneous soil layer above the bedrock. Rigid foundation with specific shape is typically assumed, in order to calculate impedance functions and wave scattering. This assumption could lead to excessive scattering of incident wave energy and underestimated structural response [12].

With increase in computer power, direct simulation of dynamic SSI using finite element method (FEM), finite difference method (FDM) and boundary element method (BEM) becomes feasible. Stamos and Beskos [13] studied dynamic response of infinitely long tunnels in elastic or viscoelastic half-space under incident seismic waves by a special direct BEM. Translational, torsional and rocking response of a building SSI system excited by plane P, SV and SH wave using FDM was recently studied by Gičev et al. [6], Gičev et al. [14], Gičev et al. [15].

For direct simulation of SSI, effective input of inclined incident seismic waves is of great importance. Many artificial boundary types have been developed by approximating the radiation condition at the finite boundaries of SSI system [7, 16–18]. Using developed viscous-spring artificial boundary, various SSI and rock-structure interaction (RSI) systems excited by inclined incident plane waves, such as tunnels [19, 20], powerhouse [21] and underground large scale frame structure (ULSFS) [22] were analyzed. In these previous studies, inclined plane waves are generally assumed to occur in homogeneous ground. The only wave reflection and refraction is considered at the ground surface, while multiple layers, usually present in realistic geological settings, were not considered. It is noted that modeling and simulation of inclined wave propagation in layered ground is more complicated because of multiple reflection, refraction, reverberation and interference at both layer interfaces and ground surface. Of interest is modeling and simulation of deeply embedded structures, that extend over multiple soil layers in depth. Inclined seismic wave field, propagating through a number of layers, will interact with the embedded structure. Embedement and stiffness of the structure will modify the seismic wave field. This effect is usually called the kinematic interaction, and applies for linear elastic SSI analysis, where kinematic and inertial interaction effects can be separated, superimposed [23].

Presented is a methodology developed to investigate influence of inclined body and surface seismic wave on linear or nonlinear earthquake soil structure interaction (ESSI) behavior of soil-structure systems. Methodology is based on Wave Potential Formulation (WPF) [24, 25] as well as Domain Reduction Method (DRM) [26]. Paper is organized as follows: Brief presentation of Wave Potential Formulation and Domain Reduction Method is given in section 2. Combined Wave Potential Formulation and Domain Reduction Method (WPF-DRM) is then verified, with select results presented in section 3.1. Following that, dynamic response of a deeply embedded small modular reactor (SMR) under inclined incident SV wave at different frequencies and inclinations is analyzed and presented in sections 3.2, 3.3 and 3.4. Findings are summarized in section 4.

2. Wave Potential Formulation – Domain Reduction Method

Presented WPF-DRM methodology consists of three main steps:

1. Analytic development of free field ground motions for a layered half space, excited by an incident, inclined plane wave. Development of this seismic wave field is relying on wave potential formulation in frequency-

wave number domain. Time domain spatially varying ground motions are then synthesized through inverse Fourier transformation.

2. Development of the Effective Earthquake Forces, from DRM formulation, is then performed using free field seismic motions developed in the previous step.

3. Earthquake Soil Structure Interaction (ESSI) analysis of the soil-structure system is then performed using effective earthquake forces that are applied to a single layer of finite elements surrounding soil-structure system, so called DRM layer. The only waves that are radiated from the soil-structure system and exit the DRM layer are due to oscillations of the structure. These outgoing waves are absorbed by damping layers.

Sections 2.1 and 2.2 below provide details of Wave Potential Formulation and Domain Reduction Method, respectively.

2.1. Wave Potential Formulation for Inclined Incident Waves in Layered Media

Considered is an inclined wave that propagates in the layered ground, as shown in Figure 1. There are n layers, with layer thickness d_m, density ρ_m, compressional wave velocity α_m and shear wave velocity β_m $(m = 1, 2, .., n)$. Focus of presented development is on inclined P and SV waves, and mode conversion between them at layer boundaries. Propagation of SH wave is simpler as there is no mode conversion, so these waves are left out of presented considerations. It is noted that the wave potential formulation presented below is general and also applicable to incident SH wave [25].

Without loss of generality, incident waves is considered to be monochromatic, single frequency, with angular frequency w and horizontal phase veloc-

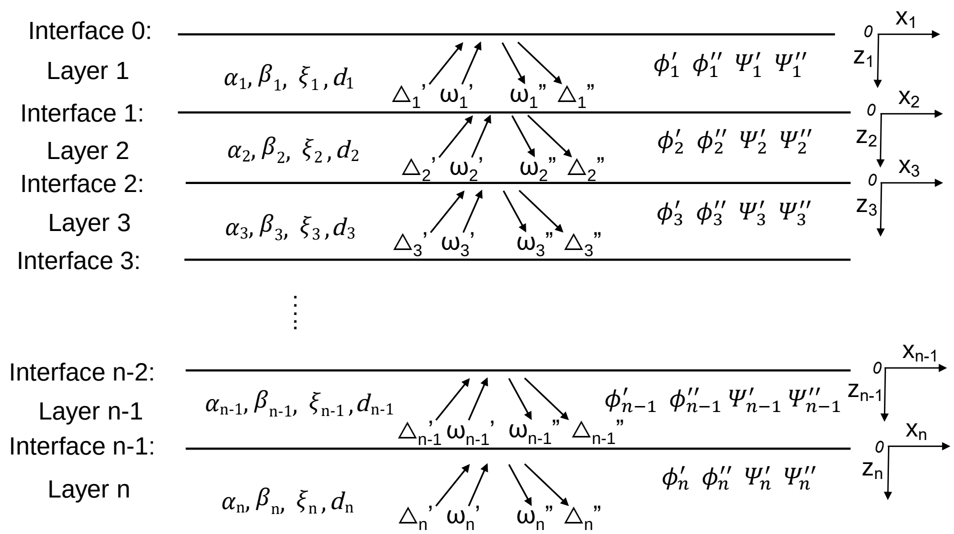

Figure 1: Layered ground and free field inclined seismic motions.

ity c. For incident waves with arbitrary time signal and multiple frequencies, free field motions can be Fourier synthesized from the monochromatic solutions.

According to Helmholtz decomposition theorem [27], the displacement from wave propagation modeled using Equation (1), for linear elastic material with Lamé constants λ and μ, can be expressed with P wave scalar potential ϕ and S wave vector potential $\mathbf{\Psi}$.

$$\rho u_{i,tt} = \mu u_{i,jj} + (\lambda + \mu)\mu_{j,ij} \tag{1}$$

This is shown in Equation 2, where ϕ is the curl free part corresponding to volumetric deformation and Ψ is divergence free part corresponding to deviatoric deformation. e_{ijk} is Levi-Civita permutation symbol [27].

$$u_i = \phi_{,i} + \Psi_{k,j} e_{ijk} \tag{2}$$

Using this approach, the unknown displacements for the m^{th} layer are simplified into incident P wave potential magnitude $\phi^{'}_{m}$, reflected P wave potential magnitude $\phi^{''}_{m}$, incident SV wave potential magnitude $\Psi^{'}_{m}$ and reflected SV wave potential magnitude $\Psi^{''}_{m}$, as shown in Equation 3.

$$\begin{aligned} \phi_m &= [\phi^{'}_{m} e^{ik(x-\gamma_{\alpha m} z)} + \phi^{''}_{m} e^{ik(x+\gamma_{\alpha m} z)}] e^{-iwt} \\ \Psi_m &= [\Psi^{'}_{m} e^{ik(x-\gamma_{\beta m} z)} + \Psi^{''}_{m} e^{ik(x+\gamma_{\beta m} z)}] e^{-iwt} \end{aligned} \tag{3}$$

In Equation 3, the horizontal wave number k is defined as $k = w/c$. The harmonic nature of the potential field is characterized by the time factor e^{-iwt}. The incident and reflected angles for P and SV wave are equal to $arccot\gamma_{\alpha_m}$ and $arccot\gamma_{\beta_m}$, where γ_{α_m} and γ_{β_m} are given in Equation 4.

$$\begin{aligned} \gamma_{\alpha_m} &= \begin{cases} \sqrt{(c/\alpha_m)^2 - 1} & \alpha_m \leq c \\ -i\sqrt{1-(c/\alpha_m)^2} & \alpha_m > c \end{cases} \\ \gamma_{\beta_m} &= \begin{cases} \sqrt{(c/\beta_m)^2 - 1} & \beta_m \leq c \\ -i\sqrt{1-(c/\beta_m)^2} & \beta_m > c \end{cases} \end{aligned} \tag{4}$$

Note that when compressional wave velocity α_m and/or shear wave velocity β_m are greater than the horizontal phase velocity c, the incidence from P or SV wave is beyond the critical angle. In that case, the incident and reflected angles for P and SV wave, γ_{α_m} and γ_{β_m} become complex numbers. The plane wave magnitude exponentially decays along the depth. To be consistent with the original formulation by Haskell [25], dilatational wave solution Δ_m and rotational wave solution ω_m are first introduced through Equation (5).

$$\begin{aligned} \Delta &= \frac{\partial u_x}{\partial x} + \frac{\partial u_z}{\partial z} \\ \omega &= \frac{1}{2}(\frac{\partial u_x}{\partial z} - \frac{\partial u_z}{\partial x}) \end{aligned} \tag{5}$$

where P wave potential magnitude ϕ_m and SV wave potential magnitude Ψ_m of m-th layer are related to dilatational wave solution Δ_m and rotational wave solution ω_m through:

$$\begin{aligned} \phi_m &= -(\frac{\alpha_m}{w})^2 \Delta_m \\ \Psi_m &= 2(\frac{\beta_m}{w})^2 \omega_m \end{aligned} \tag{6}$$

The displacements (u_x, u_y) and interfacial stresses (σ_{zz}, τ_{zx}) can be expressed using wave potential magnitudes ϕ and Ψ, through Equations (2) - (6). Similarly, the displacement and stress field of m^{th} layer can be calculated from the dilatational wave and rotational wave solutions Δ_m and ω_m as

$$\begin{aligned} u_x = \{&-ik(\frac{\alpha_m}{\omega})^2[(\Delta_m^{'} + \Delta_m^{''})cos(k\gamma_{\alpha_m} z) - i(\Delta_m^{'} - \Delta_m^{''})sin(k\gamma_{\alpha_m} z)] \\ &+2ik\gamma_{\beta_m}(\frac{\beta_m}{\omega})^2[(\omega_m^{'} - \omega_m^{''})cos(k\gamma_{\beta_m} z) + i(\omega_m^{''} + \omega_m^{'})sin(k\gamma_{\beta_m} z)]\}e^{ikx} \end{aligned} \tag{7}$$

$$\begin{aligned} u_z = \{&ik\gamma_{\alpha_m}(\frac{\alpha_m}{\omega})^2[(\Delta_m^{'} - \Delta_m^{''})cos(k\gamma_{\alpha_m} z) - i(\Delta_m^{''} + \Delta_m^{'})sin(k\gamma_{\alpha_m} z)] \\ &+2ik(\frac{\beta_m}{\omega})^2[(\omega_m^{'} + \omega_m^{''})cos(k\gamma_{\beta_m} z) - i(\omega_m^{'} - \omega_m^{'})sin(k\gamma_{\beta_m} z)]\}e^{ikx} \end{aligned} \tag{8}$$

$$\begin{aligned} \sigma_{zz} = \rho_m\{&\alpha_m^2(1 - 2\frac{\beta_m^2}{c^2})[(\Delta_m^{'} + \Delta_m^{''})cos(k\gamma_{\alpha_m} z) - i(\Delta_m^{'} - \Delta_m^{''})sin(k\gamma_{\alpha_m} z)] \\ &+4\frac{\beta_m^4}{c^2}\gamma_{\beta_m}[(\omega_m^{'} - \omega_m^{''})cos(k\gamma_{\beta_m} z) - i(\omega_m^{'} + \omega_m^{''})sin(k\gamma_{\beta_m} z)]\}e^{ikx} \end{aligned} \tag{9}$$

$$\begin{aligned} \tau_{zx} = 2\rho_m\beta_m^2\{&-\gamma_{\alpha_m}(\frac{\alpha_m}{c})^2[(\Delta_m^{'} - \Delta_m^{''})cos(k\gamma_{\alpha_m} z) - i(\Delta_m^{''} + \Delta_m^{'})sin(k\gamma_{\alpha_m} z)] \\ &+[1 - 2(\frac{\beta_m}{c})^2][(\omega_m^{'} + \omega_m^{''})cos(k\gamma_{\beta_m} z) - i(\omega_m^{'} - \omega_m^{''})sin(k\gamma_{\beta_m} z)]\}e^{ikx} \end{aligned} \tag{10}$$

Define the displacement and stress solutions at m^{th} interface as column vector $S^{(m)}$:

$$S^{(m)} = [\dot{u}_x(z_m = d_m)/c, \dot{u}_z(z_m = d_m)/c, \sigma_{zz}(z_m = d_m), \tau_{zx}(z_m = d_m)]^T \quad (11)$$

Then Equations (7) - (10) can be reduced to the following matrix notations [25]:

$$S^{(m-1)} = \boldsymbol{E_m}[\Delta_m^{''} + \Delta_m^{'}, \Delta_m^{''} - \Delta_m^{'}, \omega_m^{''} - \omega_m^{'}, \omega_m^{''} + \omega_m^{'}]^T \quad (12)$$

$$S^{(m)} = \boldsymbol{D_m}[\Delta_m^{''} + \Delta_m^{'}, \Delta_m^{''} - \Delta_m^{'}, \omega_m^{''} - \omega_m^{'}, \omega_m^{''} + \omega_m^{'}]^T \quad (13)$$

where transformation matrix $\boldsymbol{E_m}$ and $\boldsymbol{D_m}$ are given as:

$$\boldsymbol{E_m} = \begin{bmatrix} -(\alpha_m/c)^2 & 0 & -\theta_m\gamma_{\beta_m} & 0 \\ 0 & -(\alpha_m/c)^2\gamma_{\alpha_m} & 0 & \gamma_m \\ -\rho_m\alpha_m^2(\theta_m - 1) & 0 & -\rho_m c^2\theta_m^2\gamma_{\beta_m} & 0 \\ 0 & \rho_m\alpha_m^2\theta_m\gamma_{\alpha_m} & 0 & -\rho_m c^2\theta_m(\theta_m - 1) \end{bmatrix} \quad (14)$$

with $\theta_m = 2(\beta_m/c)^2$.

$$\boldsymbol{D_m} = \begin{bmatrix} -(\alpha_m/c)^2 cosA_m & i(\alpha_m/c)^2 sinA_m & -\theta_m\gamma_{\beta_m} cosB_m & i\theta_m\gamma_{\beta_m} sinB_m \\ i(\alpha_m/c)^2\gamma_{\alpha_m} sinA_m & -(\alpha_m/c)^2\gamma_{\alpha_m} cosA_m & -i\theta_m sinB_m & \theta_m cosB_m \\ -\rho_m\alpha_m^2(\theta_m - 1)cosA_m & i\rho_m\alpha_m^2(\gamma_m - 1)sinA_m & -\rho_m c^2\theta_m^2\gamma_{\beta_m} cosB_m & i\rho_m c^2\theta_m^2\gamma_{\beta_m} sinB_m \\ -i\rho_m\alpha_m^2\theta_m\gamma_{\alpha_m} sinA_m & \rho_m\alpha_m^2\theta_m\gamma_{\alpha_m} cosA_m & i\rho_m c^2\theta_m(\theta_m - 1)sinB_m & -\rho_m c^2\theta_m(\theta_m - 1)cosB_m \end{bmatrix} \quad (15)$$

with $A_m = k\gamma_{\alpha_m} d_m$ and $B_m = k\gamma_{\beta_m} d_m$.

The recurrence relation between $S^{(m)}$ and $S^{(m-1)}$ then can be established as shown in Equation 16, where it was used that $\boldsymbol{G_m} = \boldsymbol{D_m}\boldsymbol{E_m^{-1}}$.

$$S^{(m)} = \boldsymbol{D_m}\boldsymbol{E_m^{-1}} S^{(m-1)} = \boldsymbol{G_m} S^{(m-1)} \quad (16)$$

Recursively applying Equation 16 leads to Equation 17. Using the relation between displacement, stress response at $(m-1)^{th}$ interface $S^{(m-1)}$ and dilatational, rotational wave solutions $\Delta_m,\ \omega_m$, Eq. 18 bridges the gap between the upper boundary (i.e., response at ground surface $S^{(0)}$) and lower boundary (i.e., solutions of wave incident layer Δ_n and ω_n), upon which specific boundary conditions can be imposed.

$$S^{(n-1)} = \prod_{i=1}^{n-1} \boldsymbol{G_i} S^{(0)} \tag{17}$$

$$\begin{gathered} S^{(0)} = \boldsymbol{L}[\Delta_n^{''} + \Delta_n^{'}, \Delta_n^{''} - \Delta_n^{'}, \omega_n^{''} - \omega_n^{'}, \omega_n^{''} + \omega_n^{'}]^T \\ \boldsymbol{L} = (\prod_{i=1}^{n-1} \boldsymbol{G_i})^{-1} \boldsymbol{E_n} \end{gathered} \tag{18}$$

The following boundary conditions are incorporated:

1. At n^{th} layer, the incident in-plane P and SV wave potential magnitude $\phi_n^{'}$ and $\Psi_n^{'}$ are given as K_1 and K_2;

2. At the ground surface ($z = 0$), the traction is free, i.e., the third and fourth component of surface response vector $S^{(0)}$ are 0.

Therefore, the reflected dilatational wave magnitude and rotational wave magnitude can be solved using Equation 19, where $\Delta_n^{'}$ is $-K_1\omega^2/\alpha_n^2$ and $\omega_n^{'}$ is $K_2 w^2/(2\beta_n^2)$.

$$\begin{bmatrix} \Delta_n^{''} \\ \omega_n^{''} \end{bmatrix} = \begin{bmatrix} L_{31} + L_{32} & L_{33} + L_{34} \\ L_{41} + L_{42} & L_{43} + L_{44} \end{bmatrix}^{-1} \begin{bmatrix} (L_{32} - L_{31})\Delta_n^{'} + (L_{33} - L_{34})\omega_n^{'} \\ (L_{42} - L_{41})\Delta_n^{'} + (L_{43} - L_{44})\omega_n^{'} \end{bmatrix} \tag{19}$$

Finally, recurrence relation, given by Equation 20

$$\begin{bmatrix} \Delta''_{m-1} + \Delta'_{m-1} \\ \Delta''_{m-1} - \Delta'_{m-1} \\ \omega''_{m-1} - \omega'_{m-1} \\ \omega''_{m-1} + \omega'_{m-1} \end{bmatrix} = \boldsymbol{D_{m-1}^{-1}} \boldsymbol{E_m} \begin{bmatrix} \Delta''_m + \Delta'_m \\ \Delta''_m - \Delta'_m \\ \omega''_m - \omega'_m \\ \omega''_m + \omega'_m \end{bmatrix} \tag{20}$$

can be used to trace back dilatational wave magnitude Δ_m and rotational wave magnitudes ω_m for the rest $n-1$ layers. Based on solution for dilatational and rotational magnitudes for each layer, the complete displacement and stress field can be easily computed, using Equations (7) - (10).

In addition, viscosity can also be included with slight modification. Considering Kelvin-Voight viscoelastic material [28], viscosity can be handled with complex Lamé modulus and wave velocities as shown in Eq. 21, where ξ is the damping ratio.

$$G^* = G(1 + 2\xi i) \quad \beta^*_m \simeq \beta_m(1 + \xi i) \quad \alpha^*_m \simeq \alpha_m(1 + \xi i) \tag{21}$$

2.2. Domain Reduction Method

Domain Reduction Method (DRM) was originally developed for studying local topography effects on seismic motions [26, 29], while earlier work [30, 31] did note soil-structure interaction modeling as the ultimate goal. In the context of DRM, engineering system is discretized using the finite element method over interior domain Ω, within boundary Γ, containing local SSI system and reduced exterior domain Ω^+, outside of boundary Γ. The nodes of the finite element model are then placed in three categories: interior nodes, boundary nodes between domains Ω and Ω^+, on the boundary Γ, and exterior nodes in exterior domain Ω^+. Corresponding nodal displacements are denoted as u_i, u_b and u_e, for interior, boundary and exterior nodes, respectively. Boundary nodes and their connected exterior nodes form a single layer of elements, called DRM layer, surrounding the interior SSI domain. The power of DRM lies in the analytical formulation of effective seismic forces P^{eff}, given by the Equation 22.

$$P^{eff} = \begin{Bmatrix} P_i^{eff} \\ P_b^{eff} \\ P_e^{eff} \end{Bmatrix} = \begin{Bmatrix} 0 \\ -M_{be}^{\Omega+} \ddot{u}_e^0 - K_{be}^{\Omega+} u_e^0 \\ M_{eb}^{\Omega+} \ddot{u}_b^0 + K_{eb}^{\Omega+} u_b^0 \end{Bmatrix} \tag{22}$$

Effective seismic forces P^{eff} represent a dynamically consistent replacement for seismic forces at the hypocenter. Effective seismic forces P^{eff} are applied to the DRM layer, and produce the free field motions in a domain without local SSI system. The effective forces are developed from free field seismic motions, hence for free field finite element models, there are no seismic motions leaving the system. When the structure is present, during SSI analysis the only outgoing motions are related to the radiation damping of structural motions.

From Eq. 22, only free field motions (u_e^0, u_b^0) at nodes of DRM layer and element mass and stiffness matrix ($M_{be}^{\Omega+}$, $K_{be}^{\Omega+}$) of DRM layer are required to calculate effective forces P^{eff}. Free field motions developed in the previous section are used in creation of the effective seismic forces as per Equation 22.

Presented approach, using analytic solution for free field 3 component (3C) seismic motions, that feature both body and surface waves, is more efficient and straightforward than conventional substructure method. In addition to free field motions, substructure method requires to solve foundation wave scattering and impedance function, both of which are challenging tasks. It is noted that very few specific shapes of foundation, e.g., circular and rectangular shape, embedded in simplified ground conditions have been studied using sub-structuring method [8, 32–38]. For the presented approach, free field motions under inclined incident plane waves are solved using wave potential formulation. Both wave scattering and dynamic SSI are automatically handled by the time domain FEM analysis that is dynamically loaded with DRM effective earthquake forces. In addition, developed Wave Potential Formulation – Domain Reduction Method (WPF-DRM) offers advantages for solving locally inhomogeneous and nonlinear SSI problems under inclined seismic excitations [39–41].

3. Illustrative Examples

Presented WPF-DRM method is implemented in the Real-ESSI Simulator [42]. Described examples and publicly available executables for the Real ESSI sequential and parallel programs are available through Real ESSI Simulator web site `http://real-essi.info/`. All numerical examples presented here are analyzed using Real-ESSI Simulator version 20.01, in parallel computing mode, on UC Davis and Amazon Web Services parallel computers.

3.1. Free Field Modeling and Verification

Free field response of layered ground excited by an inclined incident seismic wave is used to illustrate and verify developed methodology. Analytic solutions based on Thomson-Haskell propagation matrix technique [24, 25, 43] are used for verification.

A finite element model for the free field, that is 300m wide and 200m deep, consisting of three layers, as described in Table 1, is used.

It is noted that dimension of analyzed model is 300m $\times$ 200m, however there exist additional finite elements outside this domain, for the DRM layers, as well as additional higher Rayleigh damping layers outside to damp out any outgoing waves. It is also noted that theoretically there should be no waves propagating outside of the DRM layer for a free field response. Additional

Table 1: Properties of layers: thickness d, density ρ, shear wave velocity V_s, compressional wave velocity V_p and Poisson's ratio ν.

Layer	d [m]	ρ $[kg/m^3]$	V_s $[m/s]$	V_p $[m/s]$	ν
1	50	2100	500	816.5	0.2
2	100	2300	750	1403.1	0.3
3	∞	2500	1000	2081.7	0.35

damping layers are added in order to accommodate further, non-free field model expansions and additions. Finite element size is set to 5m, and with 10 finite elements per wave length, this mesh can accurately propagate waves of up to $f = 10$Hz, for surface soil with shear wave velocity of $V_s = 500\text{m/s}^2$, as per Lysmer and Kuhlemeyer [16], Watanabe et al. [44].

A number of monochromatic, single frequency plane SV wave, represented by a cosine function, with variable inclinations $\theta = 10^o, 45^o, 60^o, 80^o$ and variable frequencies, $f = 1.0, 2.5, 5.0, 10.0$Hz, are applied to the layered ground model using developed methodology. It is noted that inclination angle θ is measured between a wave propagation direction vector and vertical axes. The incident SV wave magnitude from the depth is 0.06m and is kept the same for all the analyzed cases. Free field motions are developed and introduced into the model through WPF-DRM. Figure 2 shows snapshots of wave displacements in the model, for a wave frequency of $f = 5$Hz, for different input plane wave inclinations, $\theta = 10^o, 45^o, 60^o, 80^o$.

Figure 3 shows snapshots of wave displacements in the model, for a wave that is inclined at $\theta = 60^o$, for variable input plane wave frequencies $f = 1.0, 2.5, 5.0, 10.0$Hz.

Few notes are in order upon visual inspection of results in Figures 2 and 3.

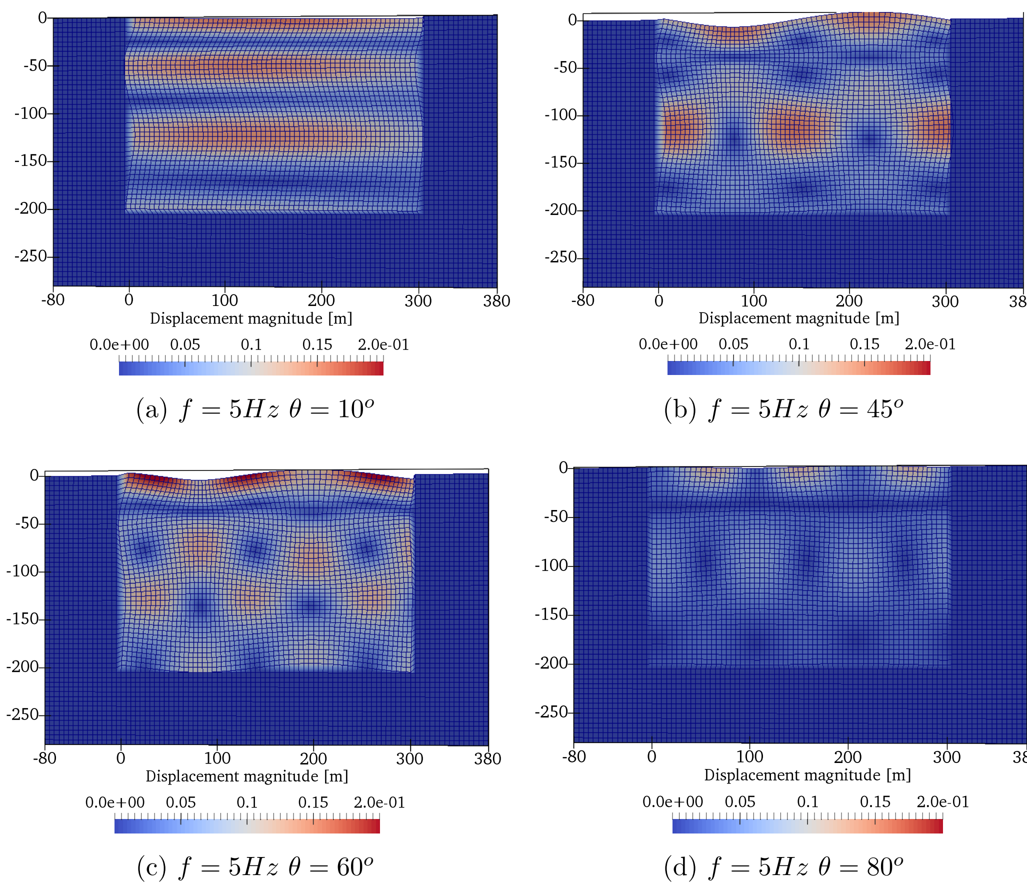

(a) $f = 5Hz\ \theta = 10^o$

(b) $f = 5Hz\ \theta = 45^o$

(c) $f = 5Hz\ \theta = 60^o$

(d) $f = 5Hz\ \theta = 80^o$

Figure 2: Displacement magnitudes for a free field response under incident SV wave, frequency $f = 5$Hz, with different incident wave inclinations: (a) $\theta = 10°$ (b) $\theta = 45°$ (c) $\theta = 60°$ (d) incident angle $\theta = 80°$.

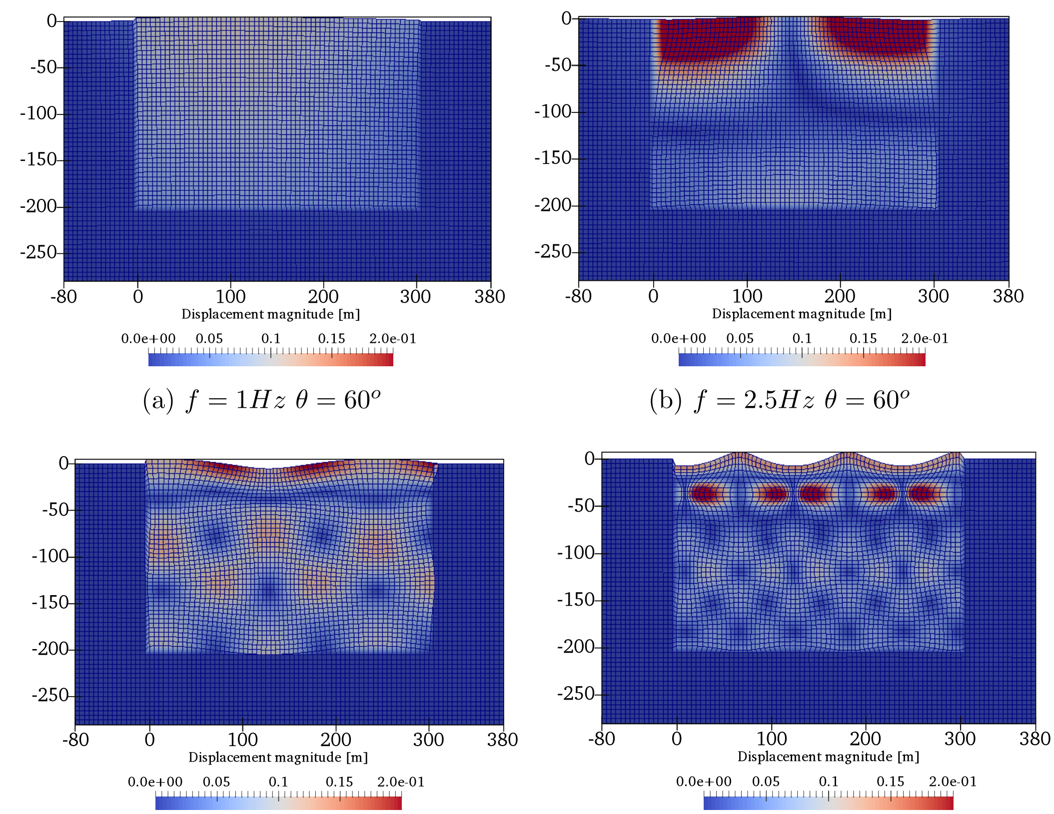

(a) $f = 1Hz$ $\theta = 60^o$

(b) $f = 2.5Hz$ $\theta = 60^o$

(c) $f = 5Hz$ $\theta = 60^o$

(d) $f = 10Hz$ $\theta = 60^o$

Figure 3: Displacement magnitudes for a free field response under incident SV wave at an angle of $\theta = 60^o$, with different frequencies: (a) $f = 1.0$Hz (b) $f = 2.5$Hz (c) $f = 5.0$Hz (d) $f = 10.0$Hz.

The outgoing waves in exterior region, outside DRM layer, are negligibly small, almost zero for all the cases. This is indeed expected, as it follows from the theory of the domain reduction method [26, 29], whereby the so called residual field (w_e) should be non-existent for free field motions, that were used to develop effective DRM forces.

Comparing free field responses for SV wave with different incident angles, Figure 2, the $\theta = 10°$ case behaves very similar to 1D vertically propagating motion field that is commonly used in engineering practice. It is noted, however that there are still vertical motions at the surface due to such almost vertical SV wave interacting with the free surface. For cases where wave inclination is more significant, for $\theta = 45°$ and $\theta = 60°$, significant surface motions are observed, with pronounced vertical and horizontal motions. When the incident wave inclination is $\theta = 80°$, seismic wave propagates almost horizontally without generating significant surface motions. It is also noted that the displacement magnitude of the seismic wave field for wave inclination case $\theta = 80°$ is much smaller than for the other cases. This is reasonable considering the site amplification for other free field cases comes, in part, from the impedance contrast of vertical wave propagation.

Results, snapshots of displacement field magnitudes for wave fields of different frequencies are shown in Figure 3 for seismic motion inclined SV wave field at $\theta = 60°$. It is noted that layer boundaries, impedance contrasts, are at -50m, and at -150m. Those layer boundaries can be visually identified from distribution of waves through model depth with positive and negative interference reflected and refracted waves within different layers of the domain.

Figures 4 and 5 compare simulated free field horizontal and vertical displacement magnitudes against corresponding analytical solutions along the depth. It is noted that acceleration magnitudes can be obtained by multi-

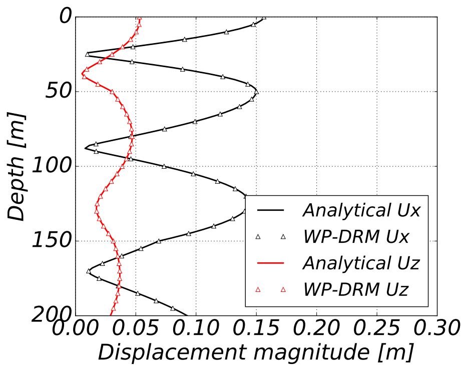

(a) $f = 5Hz$ $\theta = 10^o$

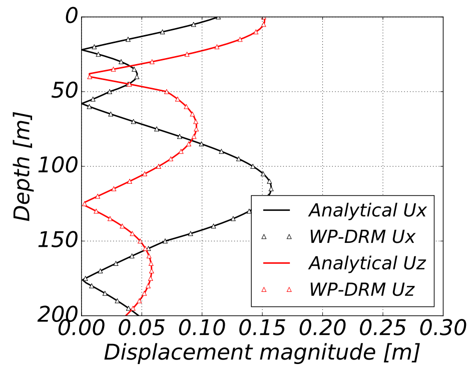

(b) $f = 5Hz$ $\theta = 45^o$

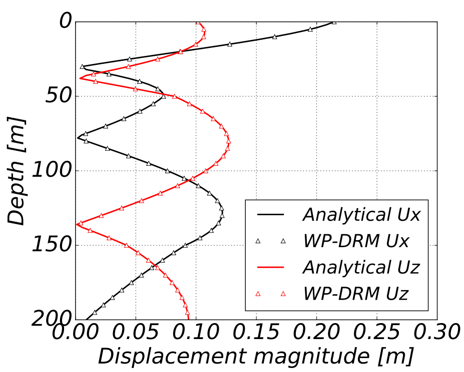

(c) $f = 5Hz$ $\theta = 60^o$

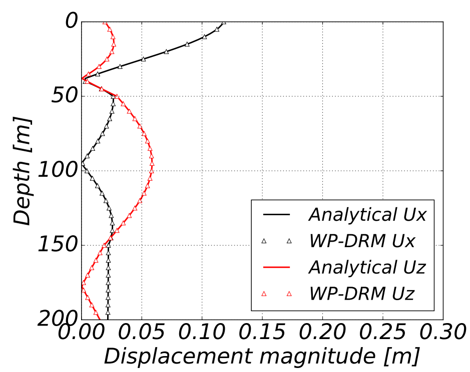

(d) $f = 5Hz$ $\theta = 80^o$

Figure 4: Verification of free field modeling under incident SV wave with different incident angles θ: (a) $\theta = 10°$, (b) $\theta = 45°$, (c) $\theta = 60°$ (d) $\theta = 80°$.

plying displacement magnitudes with w^2.

Very good agreement is observed between results given by WPF-DRM simulation and analytical solutions. Several interesting observations can also be made:

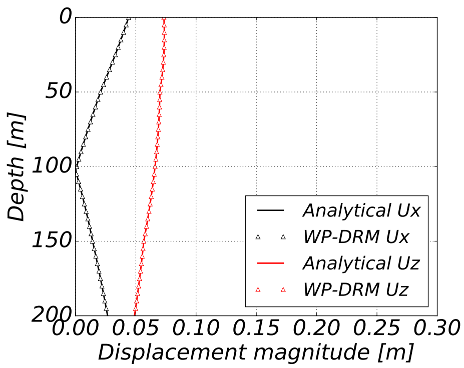

(a) $f = 1Hz\ \theta = 60^o$

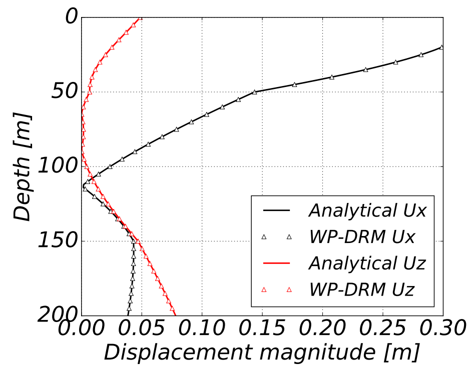

(b) $f = 2.5Hz\ \theta = 60^o$

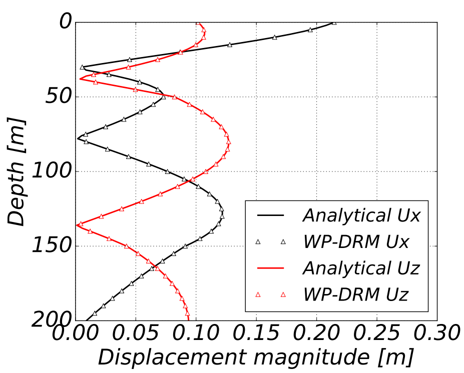

(c) $f = 5Hz\ \theta = 60^o$

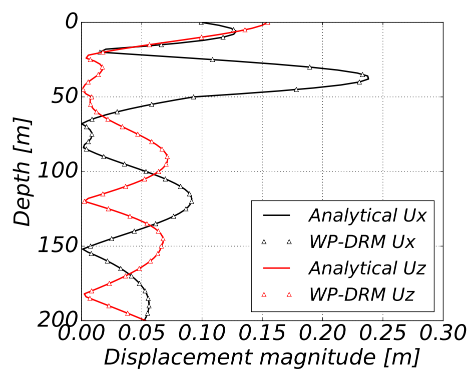

(d) $f = 10Hz\ \theta = 60^o$

Figure 5: Verification of free field modeling under incident SV wave with different frequencies f: (a) $f = 1.0$Hz, (b) $f = 2.5$Hz, (c) $f = 5.0$Hz, (d) $f = 10.0$Hz.

1. Along with the increase in frequencies, the vertical wave length becomes shorter, and that results in more wave interferences along the depth.

2. The existence of layers and interfaces at $z = -50$m and $z = -150$m complicates the spatial variation of wave field along the depth, especially for higher frequencies, $f = 5Hz$ and $10Hz$. The response curves at depths $0 \sim 50$m and $50 \sim 150$m are quite different in both amplitude and variation pattern.

3. From Fig. 4, it can be seen that inclination angle of input SV wave also plays a crucial role in the interference characteristic of inclined wave field. Periodic peaks and troughs shown in the case of $10°$ inclination are typical interference characteristics of 1D homogeneous, vertically propagating wave field. However, the interference characteristics given by other wave inclinations show significant differences. These different variation patterns along the depth, that might not make much difference for shallow founded surface structures, can result in very different seismic response for deeply embedded structures.

3.2. Deeply Embedded Soil-Structure Model

Deeply embedded structural model, a model of a Small Modular Reactor (SMR) is analyzed and used to illustrate developed methodology. The FEM model of an SMR structure embedded in layered ground is shown in Figure 6(a). The embedment depth is 36m, while the height of SMR structure above ground is 14m. Eleven representative points, point A to point K in Figure 6(b), are selected to monitor the dynamic response of SMR. The layered ground parameters are the same as those used in free field study given in Table 1.

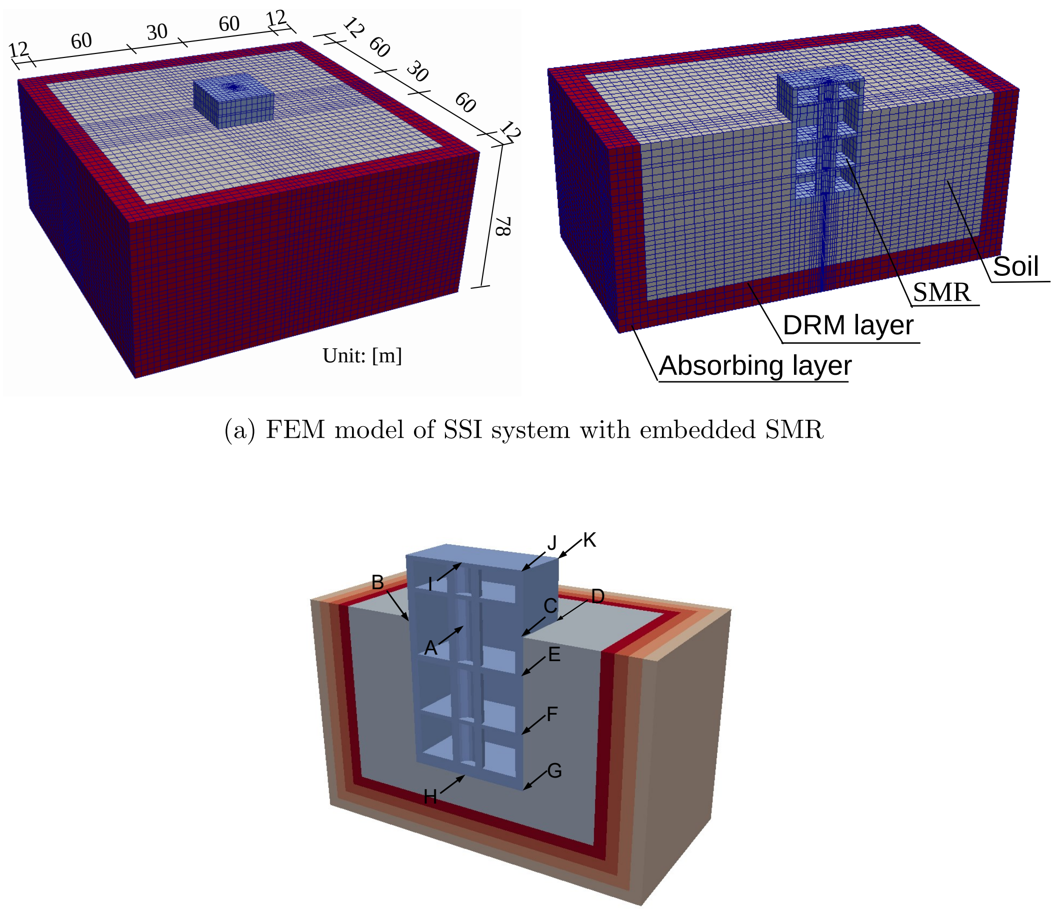

(a) FEM model of SSI system with embedded SMR

(b) Representative points configuration

Figure 6: FEM model of embedded SMR and representative points.

To proper model wave propagation, the finite element size and time step should be carefully controlled to reduce discretization errors. For linear displacement approximation within finite element, in this case eight-node brick elements, at least 10 nodes per wavelength should be used [44]. The time step length Δt is limited by Courant-Friedrichs-Lewy condition [45] for stability. In addition, following requirement needs to be met to accurately capture the propagation of wave front [46], where Δh is the mesh size and v is the highest wave velocity.

$$\Delta t < \frac{\Delta h}{v} \tag{23}$$

In this study, eight-node brick element with 4m mesh size is used for spatial discretization. The maximum frequency the model can propagate is about $12.5Hz$ considering the minimum elastic shear wave velocity $500m/s$. Time step is chosen as $\Delta t = 0.005$s. Newmark time integration method Newmark [47] is used, with small amount of numerical, algorithmic damping that is used to damp out unrealistic high frequency responses introduced by spatial discretization Argyris and Mlejnek [48]. Gradually increasing Rayleigh damping (7%, 15% and 30%) is assigned to the inner, middle and exterior part of the absorbing layers, outside of the DRM layer, to prevent reflection of radiated outgoing waves [46, 49].

3.3. SMR Excited with Inclined SV Waves

Deeply embedded SMR structure is excited with inclined plane waves, at inclination angles of $\theta = 10°, 45°, 60°$ and $80°$. Seismic wave frequency used for this set of numerical test was set at $f = 5Hz$. As described in table 1 on page 16, shear wave velocities of top 50m layer is $V_s = 500$m/s while the lower layer is 100m think and has a shear wave velocoty of $V_s = 750$m/s. Due to presence of layers, seismic wave field close to the surface is made up Rayleigh and Stoneley waves [50, 51]. It might thus be difficult to separate influence of these different surface waves the response of the SMR. For example, in Figure 2 on page 17, that shows displacement magnitudes at certain time, for different inclination of incident plane wave, Stoneley wave is apparent close to depth of 50m. In addition, Rayleigh wave is also apparent close to free field surface. Those wave fields, when applied to the SMR SSI system, produce response, at location of point A[1] on SMR structure, as shown in Figures 7 and 8.

It is noted that corresponding free field motions at the same location are also plotted for comparison. Variations of displacement magnitudes caused by different inclinations of incident SV wave are quite noticeable for vertical displacements and accelerations, while influence on horizontal displacements and accelerations is less severe. The reduction of vertical displacement and accelerations that is observed in all the four cases, is consistent with the concept of "base averaging", "ironing out" of seismic motions by Housner [52]. The most significant reduction occurs for the case of incident wave at an angle $\theta = 45°$ while little reduction is seen in the case of $\theta = 80°$.

The deformed shapes of SMR at $t = 0.4s$ for four scenarios are shown in Figure 9. In the cases of seismic waves at inclinations $\theta = 45°$ and $\theta = 60°$, rocking responses of SMR are quite evident when compared with the cases of almost vertical wave propagation ($\theta = 10°$) and almost horizontal wave propagation ($\theta = 80°$).

[1]Location of point A is in the middle of SMR structure, where center of the free field model would be, please see Figure 6 on page 23.

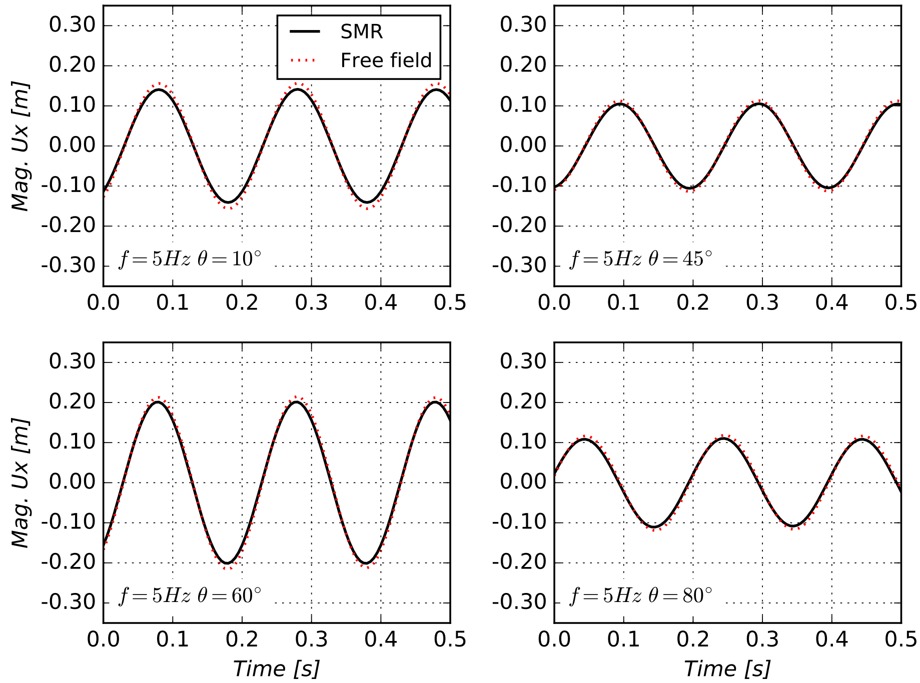

(a) Horizontal displacement

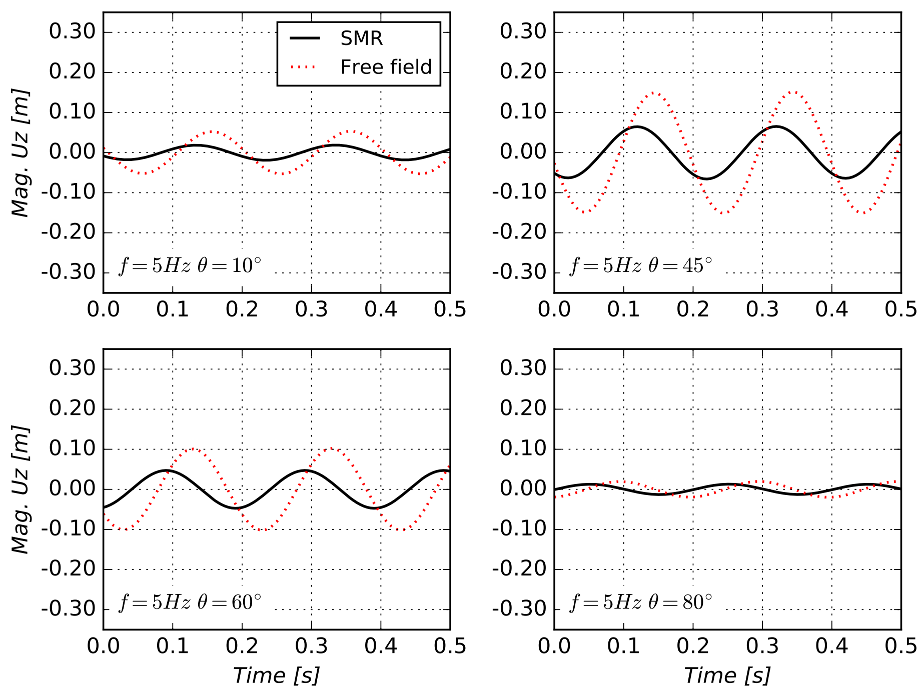

(b) Vertical displacement

Figure 7: Displacement response of point A within embedded SMR, excited by an inclined SV wave with $f = 5Hz$ and different inclination angles, $\theta = 10°, 45°, 60°$ and $80°$: (a) horizontal displacement (b) vertical displacement.

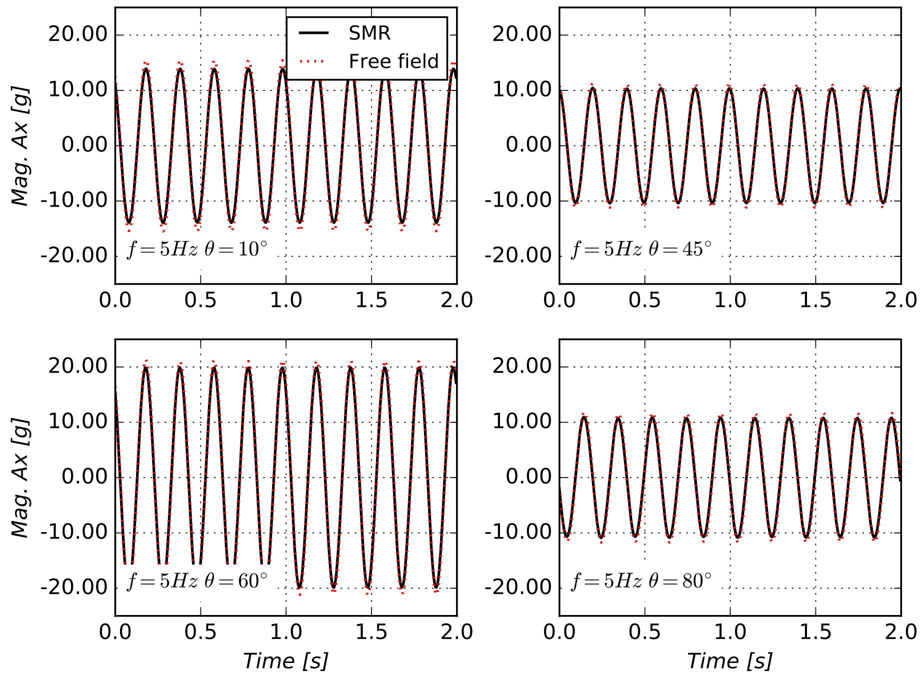

(a) Horizontal acceleration

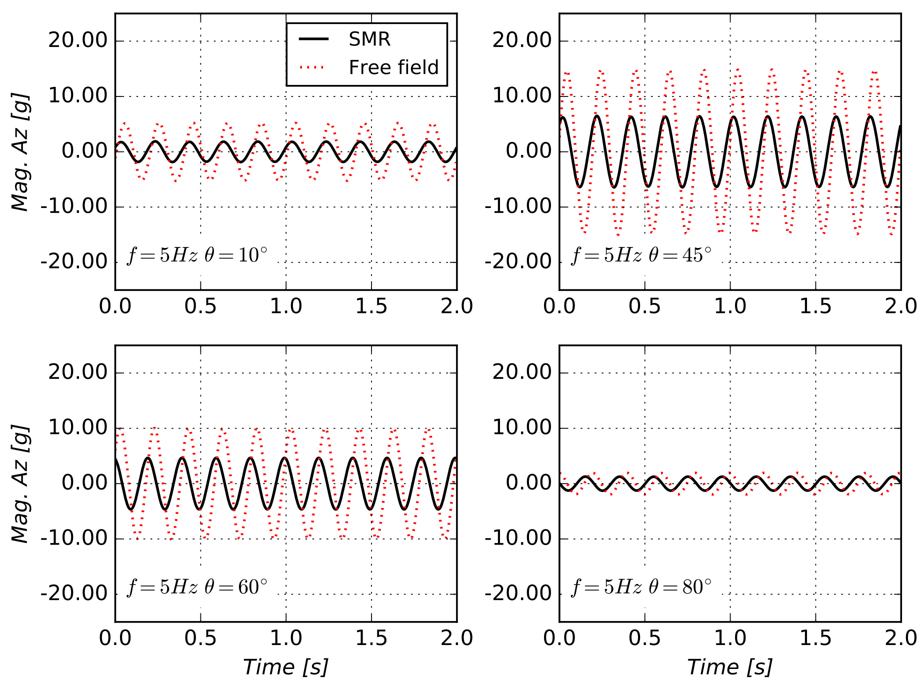

(b) Vertical acceleration

Figure 8: Acceleration response of point A within embedded SMR, excited by an inclined SV wave with $f = 5Hz$ and different inclination angles, $\theta = 10^\circ, 45^\circ, 60^\circ$ and 80°: (a) horizontal acceleration (b) vertical acceleration.

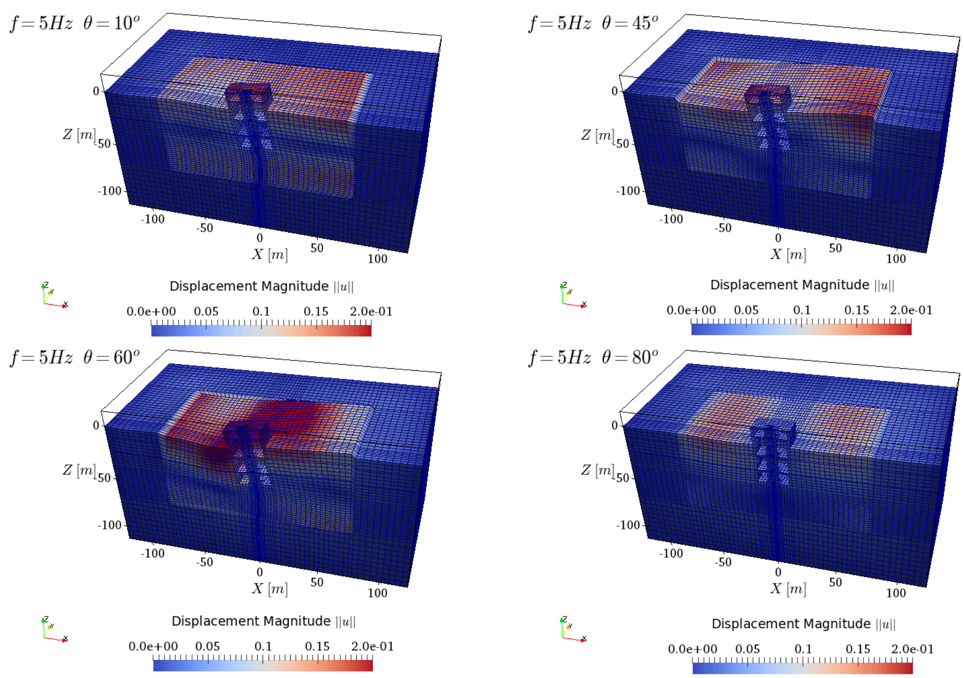

Figure 9: The deformed shapes of SMR at $t = 0.4s$ for incident SV wave at different inclinations $\theta = 10°, 45°, 60°$ and $80°$.

3.4. SMR Excited with Variable Frequency Inclined SV Waves

Keeping incidence angle constant, at $\theta = 60°$, dynamic responses of an SMR under different frequencies of SV wave ($f = f = 1Hz, 2.5Hz, 5Hz \text{and} 10Hz$) is investigated next. Figures 10 and 11, show displacement and acceleration responses at point A of SMR model.

It is noted that, again, free field response at the location of point A is also shown for comparison purposes. Significantly variation in displacement and acceleration responses are produced by incident SV wave at different frequencies. The largest horizontal displacement magnitude 0.30m is observed for the case of frequency of $f = 2.5Hz$ while the smallest horizontal magnitude of 0.047m for $f = 1Hz$. The vertical displacement responses varies from 0.02m for $f = 2.5Hz$ to 0.085m for $f = 10Hz$. SSI effects are almost negligible in the case of $f = 1Hz$ due to long horizontal wave length of 1154m. This observation follows similar observation made many years ago by Housner [52] for large stiff buildings. Both horizontal and vertical displacements of SMR overlap with corresponding free field response for $f = 1Hz$. Along with the increase of incident frequency, SSI effects become more significant, especially for the vertical components of displacement and acceleration. In the cases of $f = 2.5Hz$ and $f = 5Hz$, horizontal response of SMR is still very close to its free field counterpart, for both displacements and accelerations, however the reduction of vertical response of SMR becomes more significant for frequency of $f = 5Hz$, For relatively high frequency of $f = 10Hz$, both horizontal and vertical response of SMR are significantly different from free field modeling in both displacements and accelerations.

The spatial variation of displacements at the surface of free field model and at the same location within SMR model, along the horizontal line through SMR (i.e. $x \in [-75\text{m}, 75\text{m}], y = 0m, z = 0\text{m}$), at $t = 3.5$s are shown in Fig-

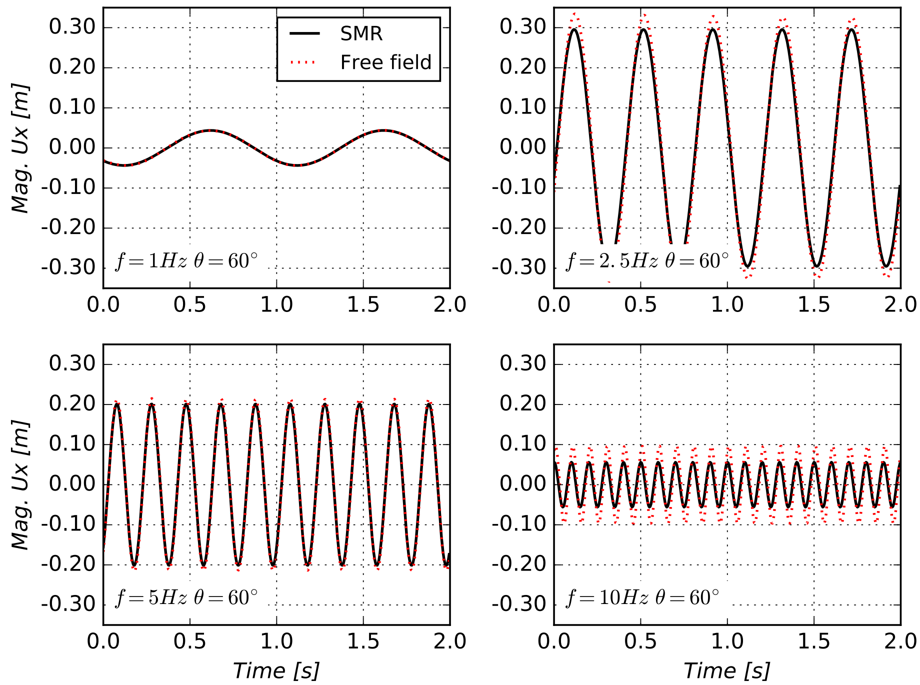

(a) Horizontal displacement

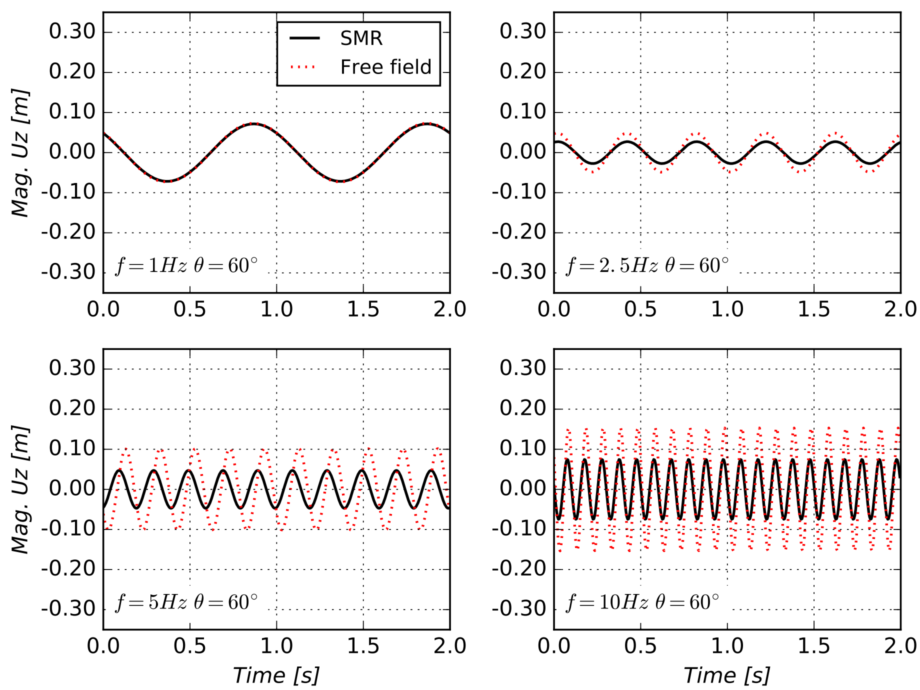

(b) Vertical displacement

Figure 10: Displacement response of point A for scenarios with different frequencies of incident SV wave: (a) Horizontal displacement (b) Vertical displacement.

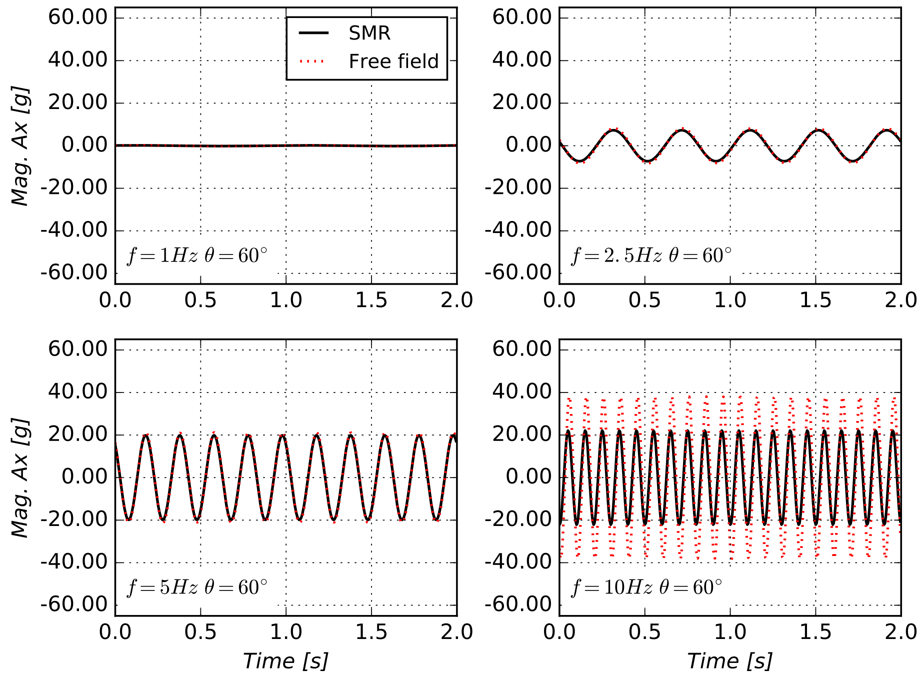

(a) Horizontal acceleration

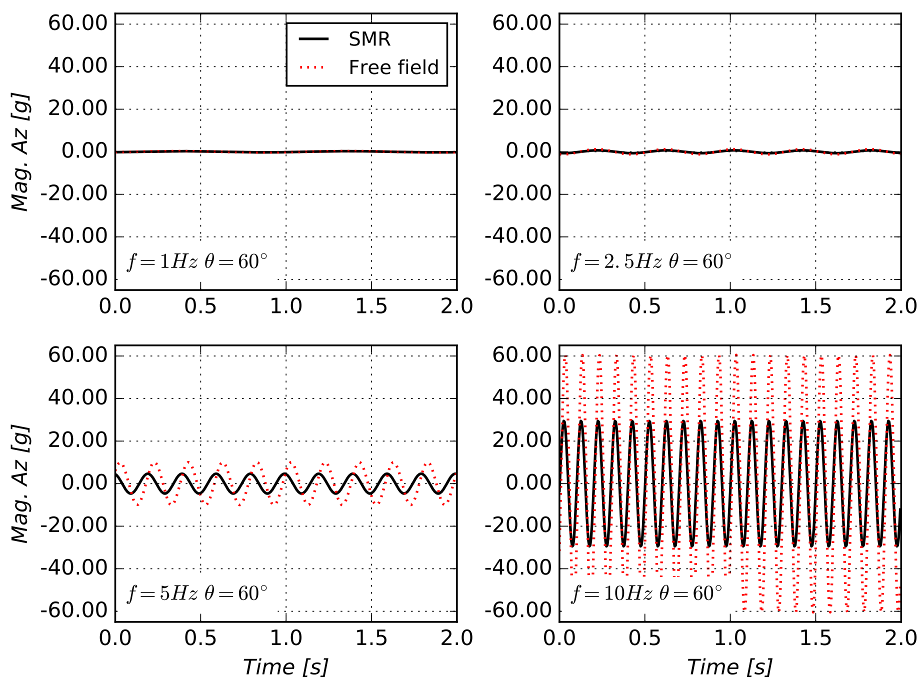

(b) Vertical acceleration

Figure 11: Acceleration response of point A for scenarios with different frequencies of incident SV wave: (a) Horizontal acceleration (b) Vertical acceleration.

ure 12. It is noted that SMR structure occupies space for $x \in [-15m, 15m]$, where flat trace of displacements within a stiff structure is observed. The

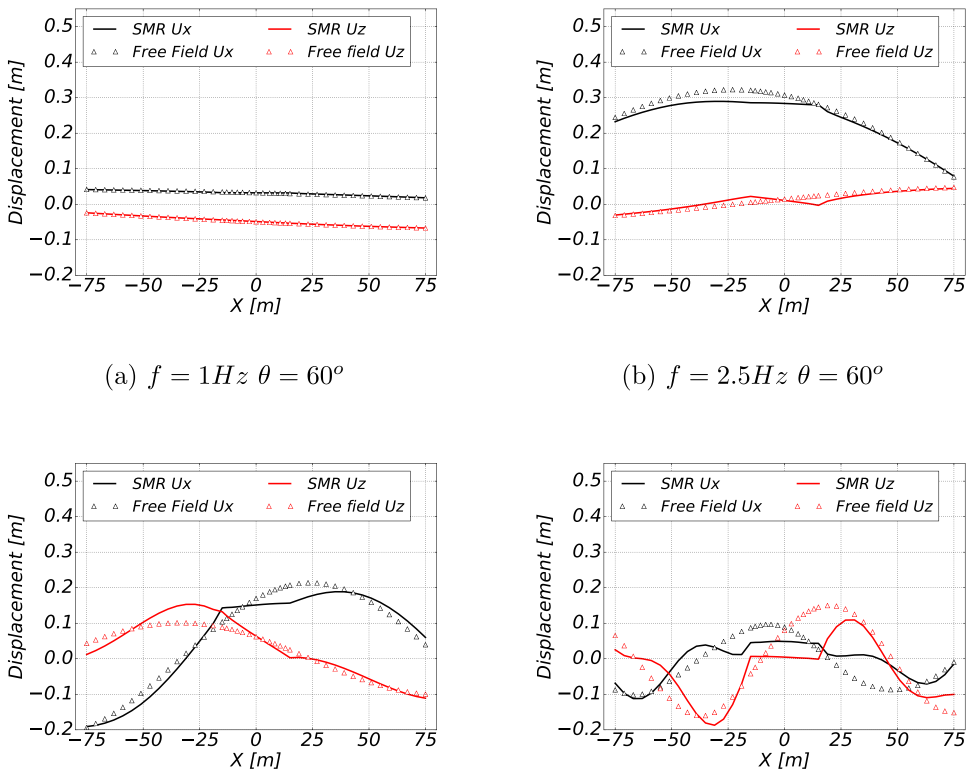

(a) $f = 1Hz\ \theta = 60^o$ (b) $f = 2.5Hz\ \theta = 60^o$

(c) $f = 5Hz\ \theta = 60^o$ (d) $f = 10Hz\ \theta = 60^o$

Figure 12: Spatial variation of displacement along the horizontal axis at $t = 3.5s$ for different incident wave frequencies (a) f$= 1Hz$ (b) f$= 2.5Hz$ (c) f$= 5Hz$ (d) f$= 10Hz$.

base slab averaging is observed for higher frequency, shorter wave length cases of f = 5Hz and f = 10Hz, while it is almost negligible for incident waves at frequencies of f = 1Hz or f = 2.5Hz due to the wavelength being longer that object size for those low frequencies.

Similar spatial variation of displacement along the transverse axis (i.e.

$x = 0m, y \in [-75m, 75m], z = 0$m) is shown in Figure 13. Since the inci-

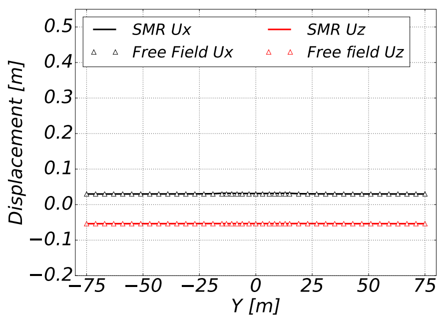

(a) $f = 1Hz\ \theta = 60^o$

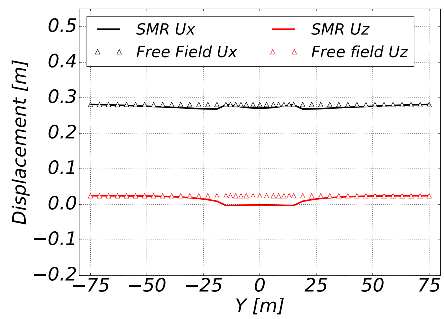

(b) $f = 2.5Hz\ \theta = 60^o$

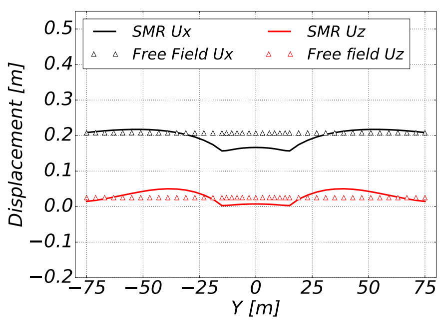

(c) $f = 5Hz\ \theta = 60^o$

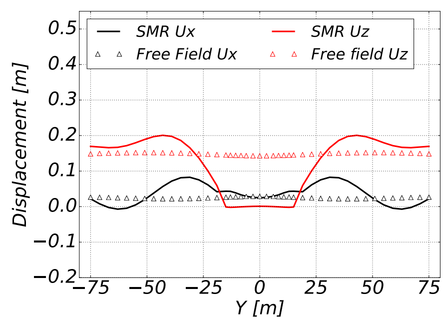

(d) $f = 10Hz\ \theta = 60^o$

Figure 13: Spatial variation of displacement along the transverse axis at $t = 3.5s$ for different incident wave frequency (a) f= $1Hz$ (b) f= $2.5Hz$ (c) f= $5Hz$ (d) f= $10Hz$.

dent SV wave propagates within the XZ plane, uniform distribution of both horizontal and vertical free field response along the transverse axis (Y axis) is expected and presented in Figure 13. However, the existence of SMR alters the original uniform distribution, and a wave field in this, out plane of polarization direction. Significant wave field disturbance effects can be observed within the structure part ($y \in [-15m, 15m]$) in the cases of medium

($f = 5Hz$) to high frequency ($f = 10Hz$). In other words, 3C dynamic response of soils surrounding the structure has been induced from 2C excitation by an SV wave due to SSI and transverse wave field disturbance effects.

Another important observation from Fig. 13(d) is that, although the reduction of displacement amplitude is observed within the structure, in locations where $y \in [-15m, 15m]$, near field motions close to the structure can be amplified, for example, motion within region $y \in \pm[25m, 50m]$ in this case. This implies that there are potentially significant structure-soil-structure dynamic effects for closely spaced structures.

The deformed shapes of SMR for four frequency scenarios at $t = 0.3s$ with different frequencies are shown in Fig. 14. The aforementioned wave field

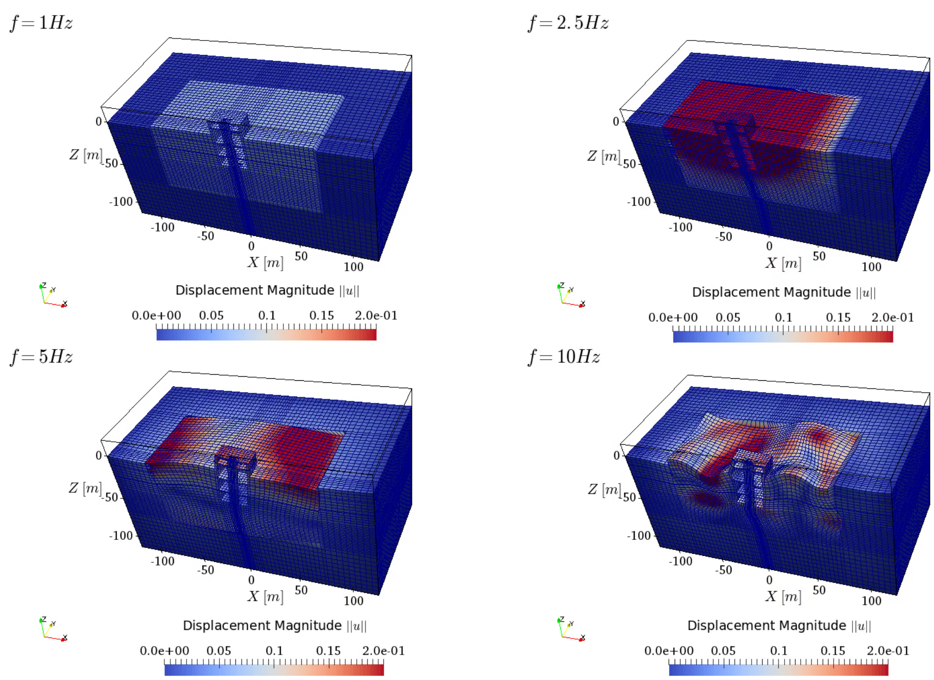

Figure 14: The deformed shapes of SMR at $t = 0.3s$ for four scenarios.

disturbance effects are clearly visible for the low wave length, high frequency case of $f = 10Hz$. The existence of local structure has significantly altered the near field seismic wave due to strong SSI effect, since wave lengths are shorter than the dominant dimension of the structure.

4. Summary

Presented was Wave-Potential-Formulation (WPF) – Domain Reduction Method (DRM) approach, called WPF-DRM, for solving Earthquake Soil Structure Interaction (ESSI) problems in layered ground excited by inclined incident seismic waves. Developed WPF-DRM methodology removes a need for many simplifying assumptions that are used in ESSI analysis, for example rigid foundation and homogeneous ground assumption. In addition, difficulties of solving for foundation wave scattering and impedance function are also circumvented. Most importantly, developed WPF-DRM method can be used with nonlinear, inelastic soil, interface and structural material behavior. WPF-DRM is verified through recoverability test (i.e., resumption behavior) of free field motions in a layered ground under incident SV waves.

Application of WPF-DRM is illustrated by analyzing a problems of an ESSI response of a deeply embedded structure, a small modular reactor (SMR). Focus was on analyzing influence of a number of differently inclined plane waves and a number of different wave frequencies, wave lengths. It is noted that free field responses for incident SV waves of varying frequencies and inclinations show significant differences between free field and SSI. For free field response, surface rolling movement pattern, Rayleigh waves are captured. This is different from typically assumed, vertically propagating wave field, and differences in SSI behavior are quite significant especially for medium and high frequency inclined incident wave. For sensitivity study, a monochromatic SSI response of SMR under incident SV wave with different frequencies and inclinations is analyzed. It is found that SSI effects are more prominent considering seismic motions with non-vertical incidence and relatively high frequency, low wave lengths. The vertical structural response is significantly influenced by the inclinations of incident wave. The vertical structure response can vary by a factor of 7 for different inclinations. Compared with almost vertical wave field ($\theta = 10°$ inclination) and almost horizontal wave field ($\theta = 80°$ inclination), more significant structural rocking response is observed in the cases of inclination $\theta = 45°$ and $\theta = 60°$. The structural response is almost identical to corresponding free field motion in the case of low frequency $f = 1Hz$ and long wavelength 1155m. As the frequency increases, structural response is different from free field counterpart because of "base averaging" of "ironing out" effects. This is particularly significant for high frequency incident wave ($f = 10Hz$) where wavelength is comparable to structural dimension, with observation of significant reduction in structural response. Observed are also wave field disturbance effects in the sense that near field motion is notably altered by the existence of embedded structure, for example, in the case of $f = 10Hz$. Presented examples provide evidence of significance of modeling uncertainties that are introduced by the assumption of uniform, vertically propagating wave field.

5. Acknowledgments

This work was supported by the University of California, by private funding sources and in small part by the US-DOE.

References

[1] MD Trifunac. A note on rotational components of earthquake motions on ground surface for incident body waves. *International Journal of Soil Dynamics and Earthquake Engineering*, 1(1):11–19, 1982.

[2] MI Todorovska and MD Trifunac. Note on excitation of long structures

by ground waves. *Journal of Engineering Mechanics*, 116(4):952–964, 1990.

[3] R Betti, AM Abdel-Ghaffar, and AS Niazy. Kinematic soil–structure interaction for long-span cable-supported bridges. *Earthquake engineering & structural dynamics*, 22(5):415–430, 1993.

[4] Roman Teisseyre, Takeo Minoru, and Eugeniusz Majewski. *Earthquake source asymmetry, structural media and rotation effects*. Springer, 2006.

[5] Muneo Hori. *Introduction to Computational Earthquake Engineering*. Imperial College Press, 2006. ISBN ISBN-10: 1848163983; ISBN-13: 978-1848163980.

[6] Vlado Gičev, Mihailo D Trifunac, and Nebojša Orbović. Translation, torsion, and wave excitation of a building during soil–structure interaction excited by an earthquake SH pulse. *Soil Dynamics and Earthquake Engineering*, 77:391–401, 2015.

[7] JP Wolf. *Dynamic Soil-Structure Interaction*. Prentice-Hall Inc, New Jersey, 1985.

[8] JE Luco and HL Wong. Response of structures to nonvertically incident seismic waves. *Bulletin of the Seismological Society of America*, 72(1): 275–302, 1982.

[9] MI Todorovska and MD Trifunac. The system damping, the system frequency and the system response peak amplitudes during in-plane building-soil interaction. *Earthquake engineering & structural dynamics*, 21(2):127–144, 1992.

[10] Maria I Todorovska. Effects of the wave passage and the embedment depth for in-plane building-soil interaction. *Soil Dynamics and Earthquake Engineering*, 12(6):343–355, 1993.

[11] Jianwen Liang, Jia Fu, Maria I. Todorovska, and Mihailo D. Trifunac. Effects of the site dynamic characteristics on soil-structure interaction (i): Incident SH-waves. *Soil Dynamics and Earthquake Engineering*, 44(0):27 – 37, 2013. ISSN 0267-7261. doi: 10.1016/j.soildyn.2012.08.013. URL http://www.sciencedirect.com/science/article/pii/S0267726112002114.

[12] Jianwen Liang, Jia Fu, Maria I Todorovska, and Mihailo D Trifunac. Effects of site dynamic characteristics on soil–structure interaction (ii): Incident p and SV waves. *Soil Dynamics and Earthquake Engineering*, 51:58–76, 2013.

[13] AA Stamos and DE Beskos. 3-d seismic response analysis of long lined tunnels in half-space. *Soil Dynamics and Earthquake Engineering*, 15 (2):111–118, 1996.

[14] Vlado Gičev, Mihailo D. Trifunac, and Nebojša Orbović. Two-dimensional translation, rocking, and waves in a building during soil-structure interaction excited by a plane earthquake P-wave pulse. *Soil Dynamics and Earthquake Engineering*, 90:454 – 466, 2016. ISSN 0267-7261. doi: http://dx.doi.org/10.1016/j.soildyn.2016.01.006. URL http://www.sciencedirect.com/science/article/pii/S0267726116000075.

[15] Vlado Gičev, Mihailo D Trifunac, and Nebojša Orbović. Two-dimensional translation, rocking, and waves in a building during soil-

structure interaction excited by a plane earthquake P-wave pulse. *Soil Dynamics and Earthquake Engineering*, 90:454–466, 2016.

[16] John Lysmer and Roger L. Kuhlemeyer. Finite dynamic model for infinite media. *Journal of Engineering Mechanics Division, ASCE*, 95 (EM4):859–877, 1969.

[17] Jingbo Liu, Yixin Du, Xiuli Du, Zhenyu Wang, and Jun Wu. 3D viscous-spring artificial boundary in time domain. *Earthquake Engineering and Engineering Vibration*, 5(1):93–102, 2006.

[18] Daniel Baffet, Jacobo Bielak, Dan Givoli, Thomas Hagstrom, and Daniel Rabinovich. Long-time stable high-order absorbing boundary conditions for elastodynamics. *Computer Methods in Applied Mechanics and Engineering*, 241-244(0):20 – 37, 2012. ISSN 0045-7825. doi: http://dx.doi.org/10.1016/j.cma.2012.05.007. URL http://www.sciencedirect.com/science/article/pii/S0045782512001557.

[19] Jing-Qi Huang, Xiu-Li Du, Liu Jin, and Mi Zhao. Impact of incident angles of p waves on the dynamic responses of long lined tunnels. *Earthquake Engineering & Structural Dynamics*, 45(15):2435–2454, 2016.

[20] Jingqi Huang, Mi Zhao, and Xiuli Du. Non-linear seismic responses of tunnels within normal fault ground under obliquely incident p waves. *Tunnelling and Underground Space Technology*, 61:26–39, 2017.

[21] Xiaowei Wang, Juntao Chen, and Ming Xiao. Seismic responses of an underground powerhouse structure subjected to oblique incidence sv and p waves. *Soil Dynamics and Earthquake Engineering*, 119:130 – 143, 2019. ISSN 0267-7261. doi: https://doi.org/10.1016/j.soildyn.2019.01.

014. URL http://www.sciencedirect.com/science/article/pii/S0267726117307935.

[22] Dapeng Qiu, Jianyun Chen, and Qiang Xu. Dynamic responses and damage forms analysis of underground large scale frame structures under oblique sv seismic waves. *Soil Dynamics and Earthquake Engineering*, 117:216–220, 2019.

[23] Steven L. Kramer. *Geotechnical Earthquake Engineering*. Prentice Hall, Inc, Upper Saddle River, New Jersey, 1996.

[24] William T Thomson. Transmission of elastic waves through a stratified solid medium. *Journal of applied Physics*, 21(2):89–93, 1950.

[25] Norman A Haskell. The dispersion of surface waves on multilayered media. *Bulletin of the seismological Society of America*, 43(1):17–34, 1953.

[26] Jacobo Bielak, Kostas Loukakis, Yoshiaki Hisada, and Chiaki Yoshimura. Domain reduction method for three–dimensional earthquake modeling in localized regions. part I: Theory. *Bulletin of the Seismological Society of America*, 93(2):817–824, 2003.

[27] George B Arfken and Hans J Weber. *Mathematical methods for physicists*. AAPT, 1999.

[28] S Chiriţă, C Galeş, and ID Ghiba. On spatial behavior of the harmonic vibrations in kelvin-voigt materials. *Journal of Elasticity*, 93(1):81–92, 2008.

[29] Chaiki Yoshimura, Jacobo Bielak, and Yoshiaki Hisada. Domain reduction method for three–dimensional earthquake modeling in localized

regions. part II: Verification and examples. *Bulletin of the Seismological Society of America*, 93(2):825–840, 2003.

[30] Jacobo Bielak and Paul Christiano. On the effective seismic input for non-linear soil-structure interaction systems. *Earthquake Engineering & Structural Dynamics*, 12(1):107–119, 1984. ISSN 1096-9845. doi: 10.1002/eqe.4290120108. URL http://dx.doi.org/10.1002/eqe.4290120108.

[31] Marco G. Cremonini, Paul Christiano, and Jacobo Bielak. Implementation of effective seismic input for soil-structure interaction systems. *Earthquake Engineering & Structural Dynamics*, 16(4):615–625, 1988. doi: 10.1002/eqe.4290160411. URL https://onlinelibrary.wiley.com/doi/abs/10.1002/eqe.4290160411.

[32] J. Enrique Luco. Impedance functions for a rigid foundation on a layered medium. *Nuclear Engineering and Design*, 31:204–217, 1974.

[33] L. H. Wong and J. Enrique Luco. Tables of impedance functions for square foundations on layered media. *International Journal of Soil Dynamics and Earthquake Engineering*, 4(2):64–81, 1985.

[34] C. B. Crouse, Behnam Hushmand, J. Enrique Luco, and H. L. Wong. Foundation impedance functions: Theory versus experiment. *Journal of Geotechnical Engineering*, 116(3):432–449, March 1990.

[35] JE Luco. Torsional response of structures for sh waves: the case of hemispherical foundations. *Bulletin of the Seismological Society of America*, 66(1):109–123, 1976.

[36] FCP De Barros and JE Luco. Dynamic response of a two-dimensional semi-circular foundation embedded in a layered viscoelastic half-space. *Soil Dynamics and Earthquake Engineering*, 14(1):45–57, 1995.

[37] JE Luco and HL Wong. Seismic response of foundations embedded in a layered half-space. *Earthquake engineering & structural dynamics*, 15 (2):233–247, 1987.

[38] Jia Fu, Jianwen Liang, and Bin Han. Impedance functions of three-dimensional rectangular foundations embedded in multi-layered half-space. *Soil Dynamics and Earthquake Engineering*, 103:118–122, 2017.

[39] Boris Jeremić, Zhaohui Yang, Zhao Cheng, Guanzhou Jie, Nima Tafazzoli, Matthias Preisig, Panagiota Tasiopoulou, Federico Pisanò, José Abell, Kohei Watanabe, Yuan Feng, Sumeet Kumar Sinha, Fatemah Behbehani, Han Yang, and Hexiang Wang. *Nonlinear Finite Elements: Modeling and Simulation of Earthquakes, Soils, Structures and their Interaction*. Self Published, University of California, Davis, CA, USA, and Lawrence Berkeley National Laboratory, Berkeley, CA, USA, 1989-present. ISBN 978-0-692-19875-9. URL: http://sokocalo.engr.ucdavis.edu/~jeremic/LectureNotes/.

[40] Hexiang Wang, Han Yang, Sumeet K. Sinha, Yuan Feng, Chao Luo, David B. McCallen, and Boris Jeremić. 3D non-linear earthquake soil-structure interaction modeling of embedded small modular reactor (SMR). In *Proceedings of the 24th International Conference on Structural Mechanics in Reactor Technology (SMiRT 24)*, Busan, South Korea, August 20-25 2017.

[41] Sumeet K. Sinha, Yuan Feng, Han Yang, Hexiang Wang, Nebojša Or-

bović, David B. McCallen, and Boris Jeremić. 3-d non-linear modeling and its effects in earthquake soil-structure interaction. In *Proceedings of the 24th International Conference on Structural Mechanics in Reactor Technology (SMiRT 24)*, Busan, South Korea, August 20-25 2017.

[42] Boris Jeremić, Guanzhou Jie, Zhao Cheng, Nima Tafazzoli, Panagiota Tasiopoulou, Federico Pisanò, José Antonio Abell, Kohei Watanabe, Yuan Feng, Sumeet Kumar Sinha, Fatemah Behbehani, Han Yang, and Hexiang Wang. *The Real-ESSI Simulator System*. University of California, Davis, 1989-2020. http://real-essi.us/.

[43] W Silva. Body waves in a layered anelastic solid. *Bulletin of the Seismological Society of America*, 66(5):1539–1554, 1976.

[44] Kohei Watanabe, Federico Pisanò, and Boris Jeremić. A numerical investigation on discretization effects in seismic wave propagation analyses. *Engineering with Computers*, 33(3):519–545, Jul 2017. ISSN 1435-5663. doi: 10.1007/s00366-016-0488-4. URL http://dx.doi.org/10.1007/s00366-016-0488-4.

[45] R. Courant and D. Hilbert. *Methods of Mathematical Physics*. Wiley, 1989. ISBN 979-0-471-50447-4.

[46] Boris Jeremić, Guanzhou Jie, Matthias Preisig, and Nima Tafazzoli. Time domain simulation of soil–foundation–structure interaction in non–uniform soils. *Earthquake Engineering and Structural Dynamics*, 38(5): 699–718, 2009.

[47] Nathan. M. Newmark. A method of computation for structural dynamics. *ASCE Journal of the Engineering Mechanics Division*, 85:67–94, July 1959.

[48] John Argyris and Hans-Peter Mlejnek. *Dynamics of Structures*. North Holland in USA Elsevier, 1991.

[49] José A. Abell, Nebojša Orbović, David B. McCallen, and Boris Jeremić. Earthquake soil structure interaction of nuclear power plants, differences in response to 3-D, 3×1-D, and 1-D excitations. *Earthquake Engineering and Structural Dynamics*, 47(6):1478–1495, May 2018. doi: 10.1002/eqe.3026. URL https://onlinelibrary.wiley.com/doi/abs/10.1002/eqe.3026.

[50] Keiiti Aki and Paul G. Richards. *Quantitative Seismology*. University Science Books, 2nd edition, 2002.

[51] Jean-François Semblat and Alain Pecker. *Waves and Vibrations in Soils: Earthquakes, Traffic, Shocks, Construction works*. IUSS Press, first edition, 2009. ISBN ISBN-10: 8861980309; ISBN-13: 978-8861980303.

[52] George W Housner. Interaction of building and ground during an earthquake. *Bulletin of the Seismological Society of America*, 47(3):179–186, 1957.